J Mater Sci: Mater Electron (2021) 32:20351–20361

Assessment of triboelectricity in colossal-surface-area-lanthanum oxide nanocrystals synthesized via low-temperature hydrothermal process

Sunil Meti[1], Hosangadi Prutvi Sagar[2], Mohammad Rizwanur Rahman[1], and K. Udaya Bhat[1,*]

[1] *Department of Metallurgical and Materials Engineering, National Institute of Technology Karnataka, Surathkal, Mangalore 575025, India*

[2] *Department of Metallurgical Engineering and Materials Science, Indian Institute of Technology Bombay, Powai, Mumbai 400076, India*

Received: 11 February 2021
Accepted: 30 June 2021
Published online: 14 July 2021

ABSTRACT

Triboelectric nanogenerators (TENGs) have marked their applications in various fields, most importantly, in medical devices. The electrical output of the TENGs mainly concentrated on parameters such as electrode separation distance, applied mechanical pressure, surface charge density, and overlapping surface area. The surface area of the active layer in TENGs plays a crucial role. Given this, the present contribution is the first report on the utilization of lanthanum oxide (La_2O_3) as an active material with a large surface area ($\sim$ 72.33 m^2/g) in TENGs. The nanocrystals of La_2O_3 have been successfully embedded into TENGs architecture through a high-quality screen-printed film with a Teflon-counter surface. The in-house test-rig of TENGs resulted in an output open-circuit voltage of 120 V and a short-circuit current of 23.7 μA. Further, the maximum power density is 7.125 W/m^2 at an external load resistance of 30 MΩ. These results suggest that La_2O_3 is a suitable contender in various self-powered devices.

1 Introduction

The increased human dependency on portable electronic gadgets resulted in the high demand for the energy sources, such as batteries and other storage devices. Thus, the demand for low powered and self-powered devices make their mark worldwide. The replacement of conventional devices along with powering sources by self-powered may address the energy crises for a large extent. In view of this, the triboelectric nanogenerators (TENGs) play a crucial role which harvests naturally occurring energy as a power source. The advantages of TENGs are not only the low cost production but also simple and economic fabrication of the devices. The triboelectric

Address correspondence to E-mail: udayabhatk@gmail.com

https://doi.org/10.1007/s10854-021-06545-7

device works on the principle of conjunction of triboelectrification and electrostatic induction [1]. The recent reports on active materials for TENGs have mainly focused to enhance the performance by morphology tuning, fabrication methods, and selecting the best materials [2–7]. The recent reports focused mainly on triboactive materials like zinc oxide (ZnO), polyvinylidene fluoride (PVDF), and polyimide aerogel [8, 9]. There were less or no reports on TENGs using La_2O_3 as active material. Hence, the study is focused mainly on TENGs based on La_2O_3.

Lanthanum has been widely explored in its compound states such as oxides, hydroxides as well as phosphate forms. Numerous techniques for synthesizing the lanthanum oxide nanoparticles have been proposed, such as thermal decomposition, homogeneous precipitation, solvothermal, hydrothermal, and other chemical routes [10]. From the literature, it is shown that there are many reports on microwave-assisted hydrothermal synthesis and surfactant-assisted La_2O_3 nanorods, nanoneedles, and nanorod bundles [10, 11]. Solution phase synthesis favors the agglomeration and spherical particle formation because of its high surface energy. To reduce the agglomeration of the 1D lanthanum oxide nanoparticles, suitable capping agents like surfactants, polymers, or templates were employed [12].

Lanthanum oxide is a ceramic material and is brittle in nature. Lanthanum and its compounds have been widely used in optical, electrical, magnetic materials, and most importantly in impurity extraction, such as arsenic (As (III)) [13, 14]. Recent literature on the La_2O_3 materials have revealed that it could be used in solid fuel cells, as a dielectric material in parallel plate capacitors and high-temperature superconductors [15–17]. Lanthanum oxide has found great attention in the area of piezoelectric materials, thermoelectric materials, automobile exhaust-gas convectors, optoelectronic devices, sensors, catalysis, and solid electrolyte [14, 18].

The exploration of such lanthanum oxide architectures have opened an area of interest for innovative ceramic–metal oxide nanoparticles with tuneable material properties like electronic, magnetic, and catalytic properties [19–21]. Further, high tribo-polarity, surface area, and dielectric constant are essential requirements for an active triboelectric material. In view of this, lanthanum oxide being a high permittivity dielectric finds a suitable place in the triboelectric series, thus, it has been utilized in the study; also, polarized nature of the lanthanum oxide favors its application in the area of self-powered devices [22–25]. Finally, the piezoelectric nature of the La_2O_3 material favors its application in the area of self-powered devices.

In this work, a single-step hydrothermal synthesis of La_2O_3 nanocrystals is presented. The processing is simple, cost effective, and demands a minimal thermal budget. The La_2O_3 nanocrystals synthesized with this technique processes uniform morphology and size distribution. The synthesized La_2O_3 nanocrystals are characterized to study its morphological and structural properties. The synthesized nanocrystals are grounded with suitable capping agent to form paste for the screen printing technique without modifying its base properties. The La_2O_3 film is fabricated using synthesized nanocrystals and suitable reagents by the screen printing technique. The prepared film is then examined to study the triboelectric properties.

2 Materials and methods

2.1 Hydrothermal synthesis of La_2O_3 nanocrystals

A known weight of (1.4 g) cetyltrimethylammonium bromide (CTAB) is added to 100 ml of de-ionized (DI) water. The solution is stirred vigorously for a few minutes. Then, 3 g of lanthanum chloride ($LaCl_3$) salt is added to the solution and stirred continuously using magnetic bar. 3 ml of 25% ammonia (NH_3) solution is added drop-wise to the solution to maintain a basic pH ranging between 9 and 10. The resultant solution is stirred for 12 h and made in to colloidal dispersion with a translucent appearance. The prepared solution is poured into 200 ml stainless steel autoclave and kept in an oven at 100 °C for 48 h. The products obtained post heat treatment is then rinsed with DI water and ethanol several times to annihilate the residuals. Finally, the La_2O_3 nanocrystals are subjected for drying in an oven at 80 °C for 24 h. The dried product-La_2O_3 is stored in an air-tight bottle to avoid moisture contamination.

2.2 Screen printing of La_2O_3 film

45 weight percent (45 wt%) of the as-synthesized La_2O_3 nanocrystals are mixed with 5 wt% of

ethylcellulose binder and 50 wt% of terpinol solvent. The mixture is then grounded rigorously in Mortar-pestle for 30 min to get high viscous agglomeration-free La_2O_3 screen printable paste. The mask for screen printing is created using a screen with #120 mesh. The snap-off distance of 5–10 mm is maintained to facilitate the quick release of the screen. The copper adhesive tape cleaned with isopropyl alcohol, acetone, and DI water is used as a substrate for screen printing. Here, the copper adhesive tape is flexible, which helps in device fabrication and testing, and also acts as an electrode. The films are then dried under infrared (IR) radiation for three to four hours to ensure complete evaporation of the solvent.

2.3 Characterization

The X-ray diffractometry (XRD, make-JEOL-JPZ-8 with a copper target (CuK_α = 1.54 Å)) is used for the examination of phase purification of the La_2O_3 nanocrystals. The chemical nature of La_2O_3 nanocrystals is studied by using X-ray photoelectron spectroscopy (XPS, Kratos Analytical, UK, monochromatic $AlK_\alpha \sim 1486.6$ eV as X-ray source and XPS; PHI5000VersaProbeII). Prior to the XPS measurements, the sample is treated under argon gas to eliminate the surface impurities. The calibrations of all the XPS data are performed with the standard reference carbon 1*s* (C 1*s*) peak at 284.7 eV, and ± 0.2 eV of accuracy is maintained for measuring the binding energies. The deconvolution of oxygen 1*s* (O 1*s*) and lanthanum 3*d* (La 3*d*) is performed after the subtraction of the background using Shirley function. Further, the addition of synthetic peaks is performed using Gaussian–Lorentzian peak function with area resolution of 1 eV. The nature and surface morphologies of the La_2O_3 nanocrystals are examined by using field emission scanning electron microscopy (FESEM, make-JEOL-JSM-6380LA, Tokyo, Japan) and transmission electron microscopy (TEM, JEOL-JEM-2100, Tokyo Japan). A very minute amount of La_2O_3 nanocrystals is dispersed in ethanol and a drop of prepared colloidal solution is poured on carbon-coated copper grid. Finally, the grid is dried under bulb (60 W). The grid containing La_2O_3 nanocrystals is then subjected for TEM examination. The Fourier transform infrared (FTIR, make-JASCO-4200 spectrometer, in KBr mode) is used to study the quality and the formation of La_2O_3 nanocrystals. The Brunauer–Emmett–Teller (BET) apparatus is used for the calculation of specific surface area of La_2O_3 nanocrystals following the standard protocols at 77 K. Prior to the BET measurements, the La_2O_3 nanocrystals are degassed in the presence of flowing N_2 at 300 °C for 12 h [26].

To evaluate the triboelectric performance, the screen-printed film is tested in an in-house built motorized fixture as shown in Fig. 1 and Fig. S1. The dimension of the screen-printed La_2O_3-TENG device is (2.5 cm × 2.5 cm). Teflon is used as a counter surface for testing the La_2O_3-TENG device, since it is fluorine rich, leading to high electronegativity. The thickness of the Teflon used is 0.25 mm. Before the measurement of triboelectric response, the La_2O_3 screen-printed film thickness is measured to be 10 µm with average surface roughness of 0.25 µm (Fig. S2). While testing, the fixture is operated at around 15 Hz with applied maximum load of approximately 300 g at the heterojunction. The electrical parameters (i.e., voltage and current) are logged using an oscilloscope (Tektronix DPO 2014B) and Keithley parameter analyzer (4200 s), respectively.

3 Results and discussion

3.1 Surface morphology of La_2O_3 nanocrystals

The micrographs of La_2O_3, captured from a scanning electron microscope (Fig. 2a–b) depict the rod-like morphology. The synthesized La_2O_3 nanocrystals are uniform in size and shape, showing its homogeneous formation during the synthesis. The micrographs at different locations present the uniform morphology with dimensions varying in few hundreds of nanometers.

The diameter of the La_2O_3 nanocrystals is in the range of 5 to 30 nm and length is 100 to 300 nm (Fig. 2a, b). Figure 2c shows the TEM micrograph of the La_2O_3 nanocrystals, corresponding high-resolution image (Fig. 2d), and SAED ring pattern (Fig. 2e). The TEM analysis shows the crystalline structure of La_2O_3. The interplanar spacing is 0.334 nm (from Fig. 2d). The ring pattern with intense spot is shown in Fig. 2e, the La_2O_3 nanocrystals showed the intense diffraction spots suggesting the particles formed.

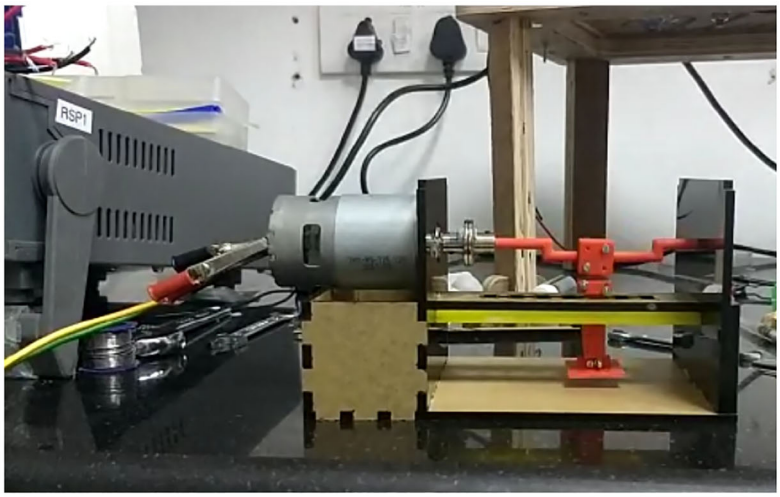

(a)

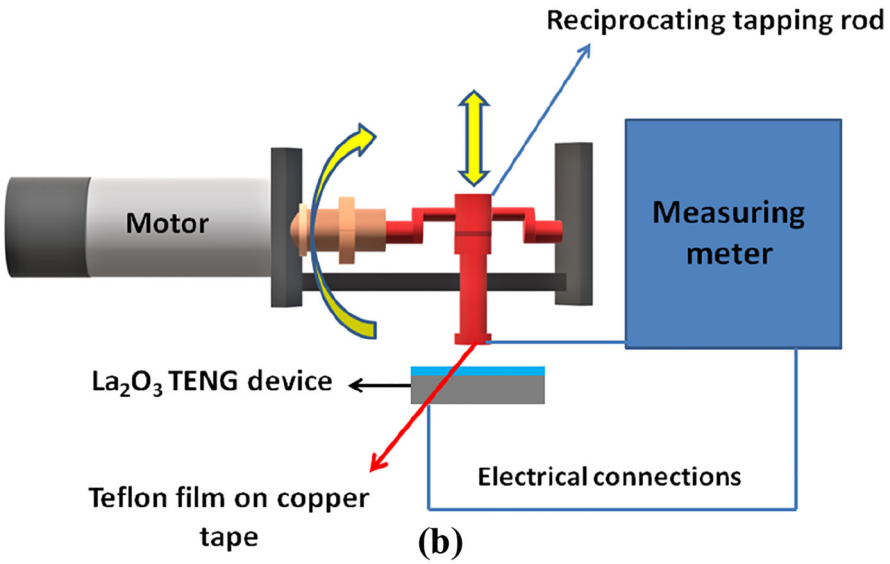

(b)

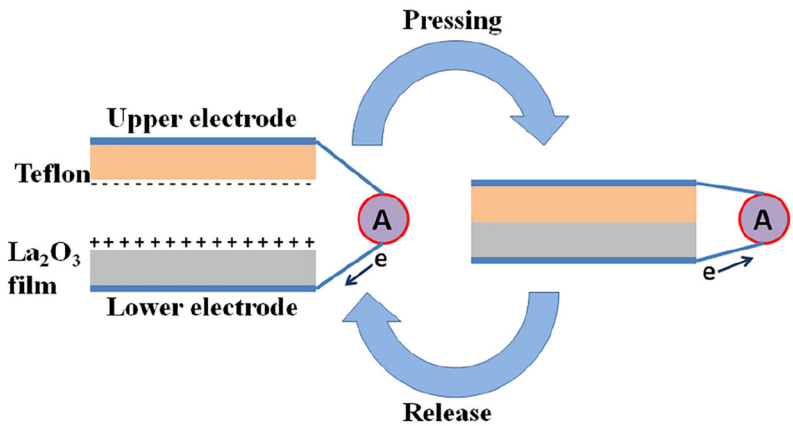

(c)

Fig. 1 **a** Image, **b** schematic representation of a motorized fixture for testing, and **c** working principle of contact-separation mode of triboelectric response of La_2O_3 film

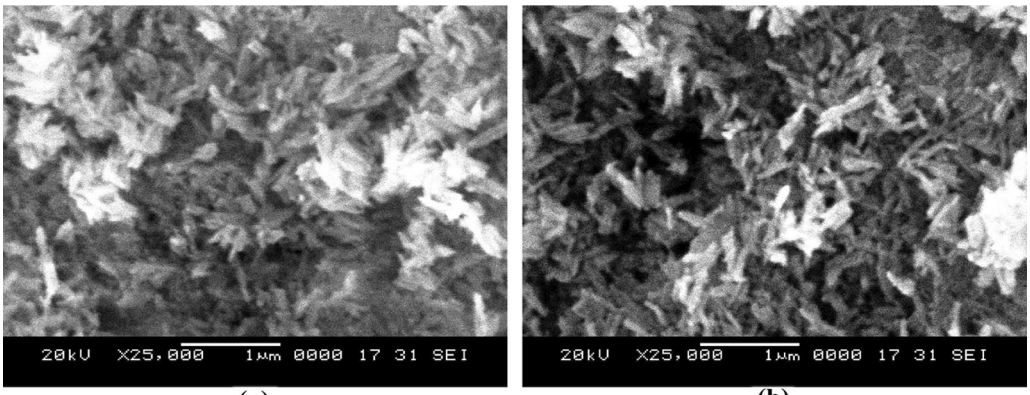
20kU X25,000 1µm 0000 17 31 SEI
20kU X25,000 1µm 0000 17 31 SEI

(a) (b)

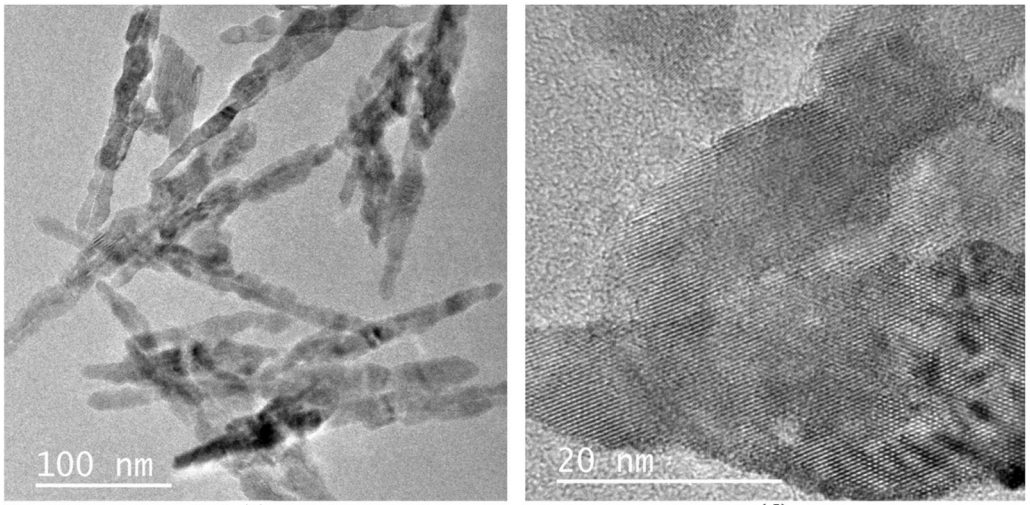
100 nm
20 nm

(c) (d)

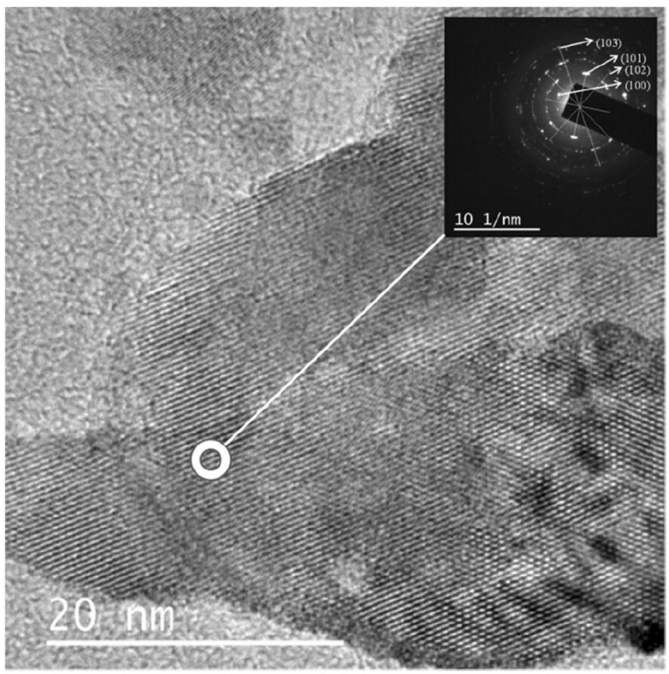
(103)
(101)
(102)
(100)
10 1/nm
20 nm

(e)

◀**Fig. 2** Morphology of La_2O_3 nanocrystals captured using, **a**, **b** SEM, **c** TEM, **d** corresponding magnified high-resolution micrograph and **e** selected area electron diffraction (SAED) ring depicting the polycrystalline nature of La_2O_3 nanocrystals

3.2 Crystal structure of La_2O_3 using XRD

The XRD of hydrothermally synthesized La_2O_3 nanocrystals is shown in Fig. 3a. The synthesized La_2O_3 nanocrystals are of high purity and pattern indexed with hexagonal phase (space group *P-3m1*, cell constant $a = 3.9397$ Å, $b = 3.9397$ Å, and $c = 6.1359$ Å, ICDD No. 83-1344) [27] (Fig. 3b). The spacing of crystal planes "*d*" calculated from the Bragg's equation ($2d \sin \theta = n\lambda$) is found to be 0.3347 nm. The magnitude of "*d*" is in good agreement with the *d*-spacing from TEM fringe pattern. The average crystallite size of La_2O_3 nanocrystals estimated from the Scherrer equation is found to be 36 nm [19].

The sharp diffraction peaks at respective Bragg angles indicate that the high crystallinity is achieved at considerably low temperatures. Thus, both morphological and structural analyses conclude the quality of the synthesized nanocrystals. Also, the broad peaks with large FWHM depict the nanocrystalline nature, which is in good agreement with high-resolution TEM studies presented in Fig. 2c–d.

3.3 Chemical composition of La_2O_3 nanocrystals using XPS

Further, the La_2O_3 sample is subjected for XPS study to examine the composition. All the binding energy data of La_2O_3 sample obtained from the XPS analysis are corrected according to the standard referencing C 1*s* peak (284.7 eV). From Fig. 4a, the XPS survey spectrum shows only the presence of two metal elements, lanthanum and oxygen. The survey also shows that there is no presence of other metal elements on the surface of La_2O_3 sample. The presence of minor C 1*s* peak (Fig. 4a) is due to the surface-adsorbed carbon atoms/molecules during the hydrothermal synthesis. The binding energy at 833.6 and 850.1 eV are indexed to the presence of La $3d_{5/2}$ and La $3d_{3/2}$, respectively, as shown in Fig. 4b. The binding energy peak at 529.5 eV, in Fig. 4c, is indexed to the O^{2-} in the La_2O_3 crystal. It is also seen that the

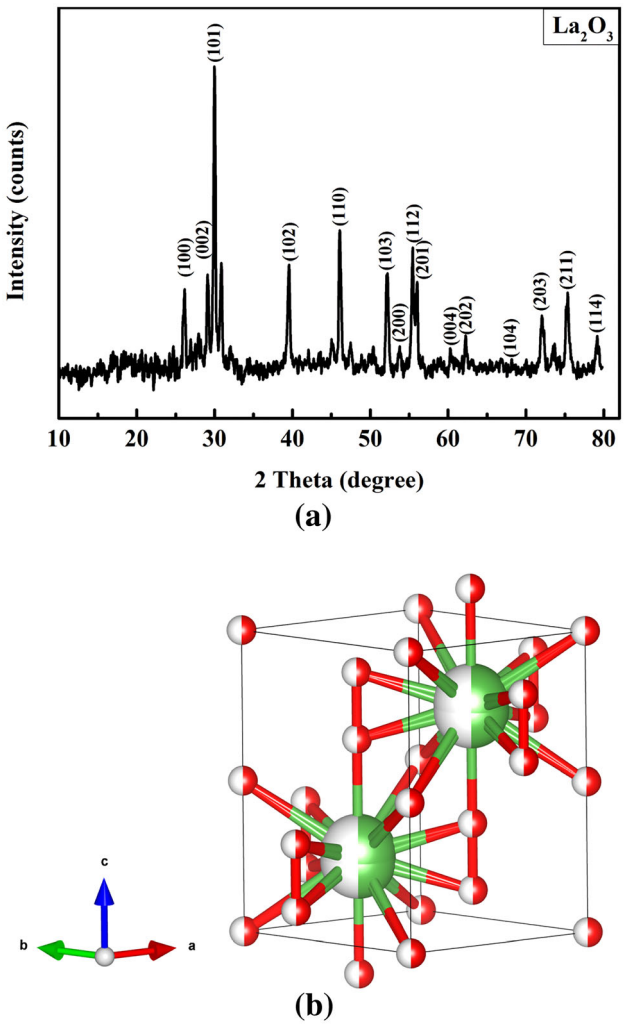

Fig. 3 **a** The XRD spectrum and **b** crystal structure of La_2O_3 (green-lanthanum and red-oxygen) of hydrothermally synthesized La_2O_3 nanocrystals

O 1*s* profile is asymmetric indicating the presence of two oxygen species in the nearby region.

3.4 BET surface area analysis

Brunauer–Emmett–Teller (BET) nitrogen gas adsorption–desorption measurements are used to find out the specific surface area of the La_2O_3 nanocrystals. The isotherm shows that the particles are porous (Fig. 5). The specific surface area of La_2O_3 from the BET apparatus is measured to be 72.33 m^2/g. The value is predominant compared to already published literatures [28–30]. Table 1 represents some of the already published surface area values of the La_2O_3 nanocrystals.

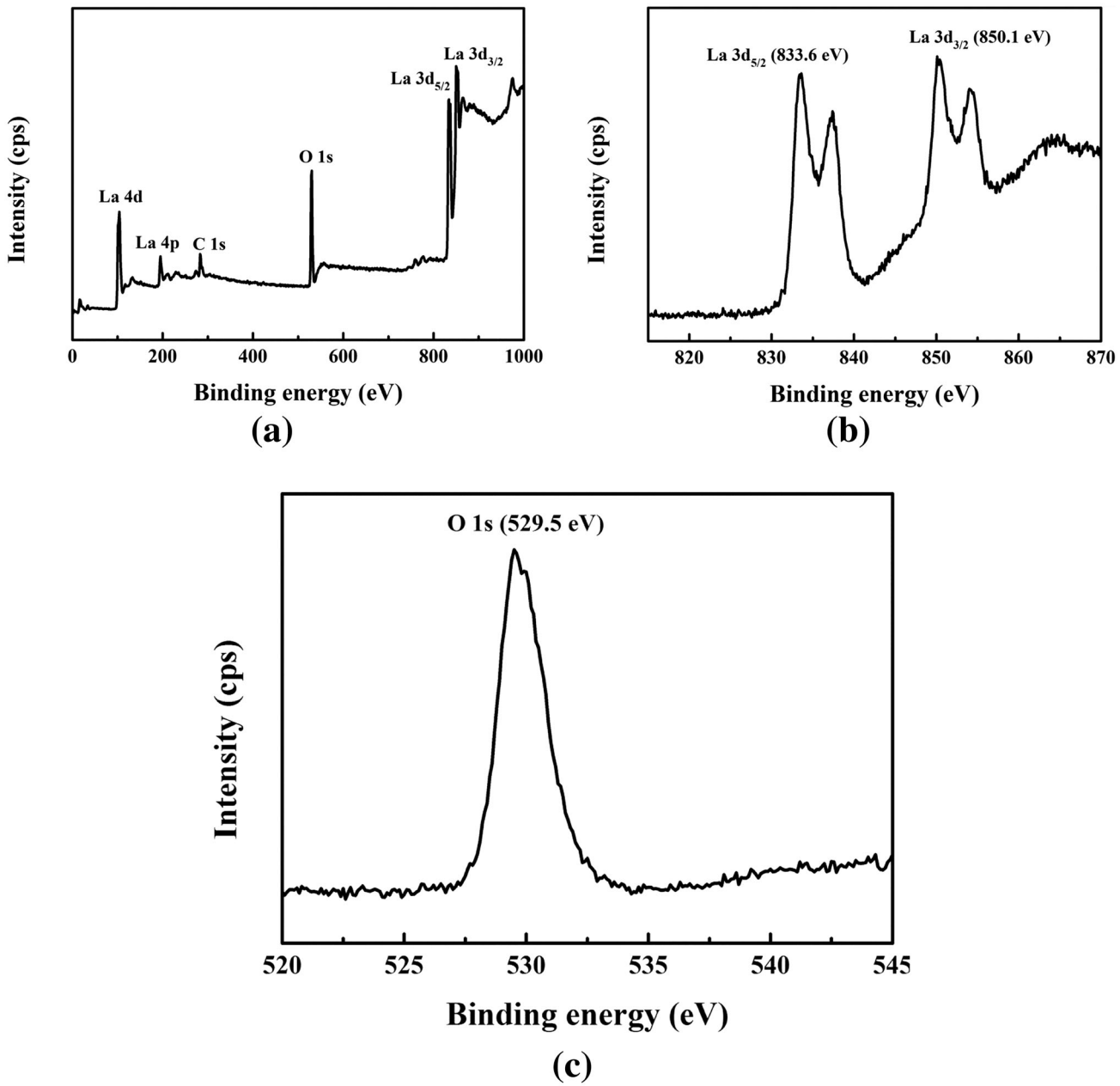

Fig. 4 XPS survey spectra of the La_2O_3 showing both **a** low- and high-resolution scans, **b** La 3*d* region, and **c** O 1 *s* region

3.5 Identification of chemical bonding by FTIR

The FTIR spectrum is recorded to show the functional groups of the La_2O_3 nanocrystals (as shown in Fig. 6). The stretching vibration of O–H bond at 3427 cm^{-1} and the bending vibration of H–O–H absorption peak at 1631 cm^{-1} are due to the presence of moisture in La_2O_3 sample [31]. The absorption bond at 3608 cm^{-1} is assigned to the presence of bond tension in hydroxyl groups of lanthanum oxide. Further, the bands at 1483 cm^{-1} and 1440 cm^{-1} are attributed to asymmetric stretching mode of the C–O bond [27]. The absorption bands at 858 and 657 cm^{-1} are assigned to bending out of plane vibrations and La–O stretching vibration, respectively [32].

3.6 Output characteristics of triboelectric nanogenerators

To evaluate the maximum power generated by the device, TENG device is connected to an electrical

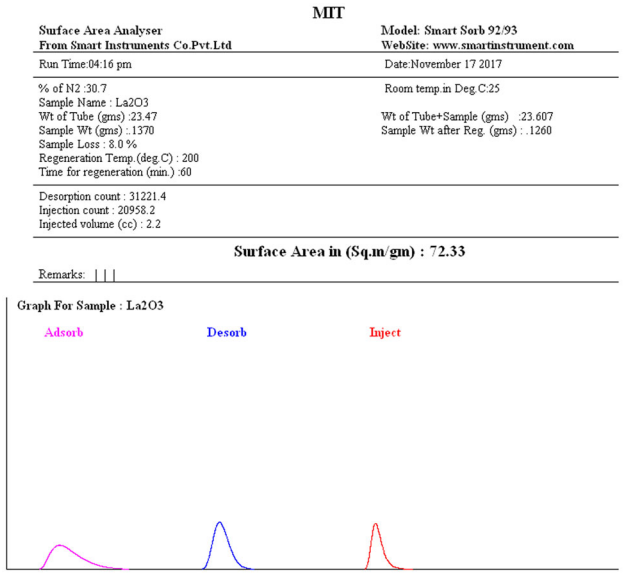

Fig. 5 Nitrogen (N_2) adsorption/desorption isotherms for La_2O_3 nanocrystals

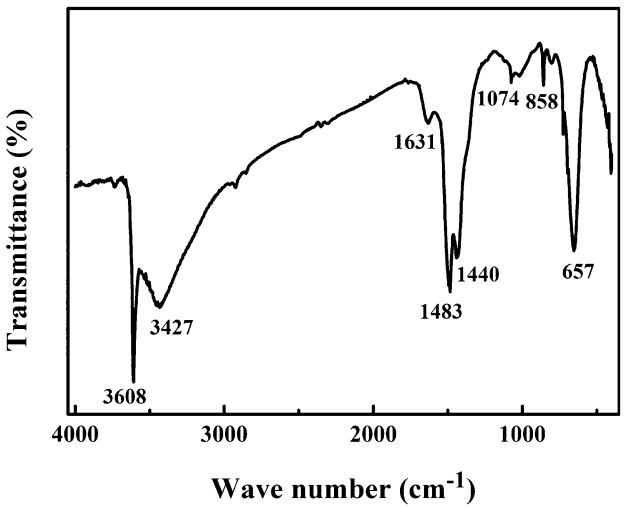

Fig. 6 FTIR analysis of La_2O_3 nanocrystals

load (resistor)s [33]. The obtained voltage is as shown in Fig. 7. The resistance value is swept from 0 to 50 MΩ. Respective voltage and current produced by the La_2O_3-TENG device are plotted against the external load resistance. The product of the same (i.e., voltage and current) gives the power value as is found to be maximum at the point where current and voltage intersect each other at 30 MΩ.

The current amplitude reduces with growing external load resistance owing to resistive loss, during which the voltage increases. Oscilloscope is used to record the voltage and current generated by La_2O_3-TENG device. The performance of the device is tested by tapping the TENG using the motorized fixture (Fig. 1). The phenomenon of chemisorptions on the surface of teflon and La_2O_3 film surface of molecular oxygen species results in resistivity changes of triboelectric material [34, 35]. When Teflon and La_2O_3 nanorods film come into contact, spontaneous polarization occurs [36]. This results in the dipole moments on Teflon film and La_2O_3 surface and thus voltage generates. The open-circuit voltage and short circuit produced by the La_2O_3-TENG device is 120 V and 23.7 μA. The device yields a maximum power of 2.85 mW at an external load resistance of 30 MΩ (Fig. 7). The corresponding power density of the La_2O_3-TENG device is calculated to be 7.125 W/m^2.

The self-powered (TENG) vibration sensors help in predicting the maintenance of industrial machineries. Recent literatures suggest that the materials with high dielectric constant and highly negative triboelectric polarity are selected for the TENG devices. The recent reports suggest that the La_2O_3 is proven to be a material with high dielectric permittivity and PTFE is having a high triboelectric negative polarity (Fig. S4). The La_2O_3-based TENG device here is tested for the power density and longer life cycle of the materials. It is proved from the testing that the fabricated device is capable of generating enough power to drive the self-powered vibration sensors. The power output of the La_2O_3-TENG devices can be

Table. 1 Specific surface area of La_2O_3 nanocrystals published by researchers

Si. no	Method	Specific surface area (m^2/g)	References
1	La_2O_3-SiO_2—sol–gel and combustion method	16.7	[30]
2	La_2O_3—homogeneous precipitation method	18.76	[29]
3	La_2O_3—reverse micelle method	12.5	[37]
4	La_2O_3—Hydrothermal method	35.61	[38]
5	Precipitation method	34	[39]
6	Physical mixing and impregnation method	19.44	[40]
7	Hydrothermal method	72.33	Present work

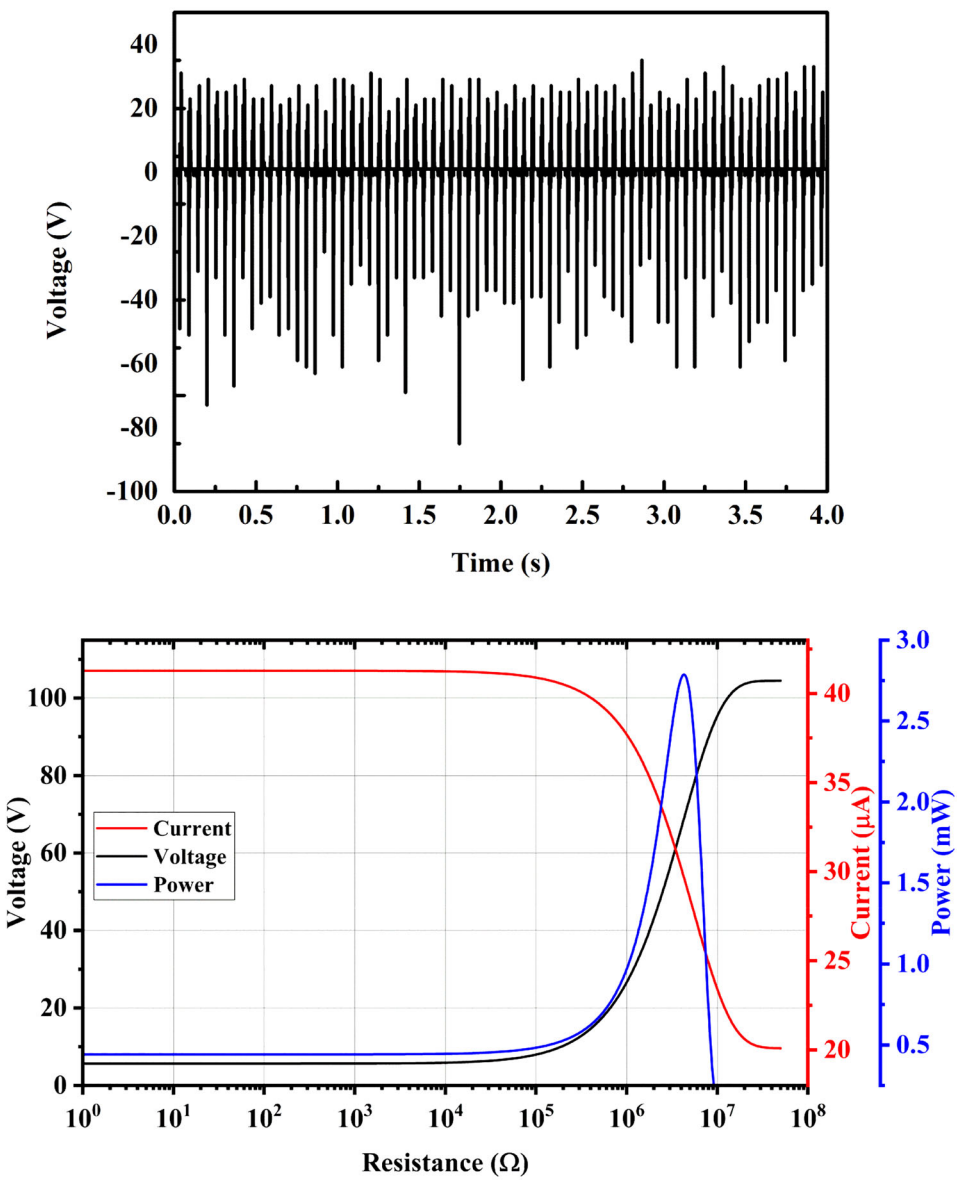

Fig. 7 The characteristic electrical output of the La_2O_3 triboelectric device showing its dependency of voltage and current output on external load resistance

improved by following many modifications and engineering of the materials. The power output can be enhanced by physical, chemical, and hybrid modifications of La_2O_3 film [17]. These methods enhance the power output of the La_2O_3-based TENG devices. The lanthanum oxide nanoparticles as a triboactive material along with the PTFE materials have proven to be competitive enough to be used in the self-powered vibration sensors.

4 Conclusions

The synthesis of high surface area (~ 72.33 m^2/g) La_2O_3 nanocrystals using the hydrothermal technique is presented with its direct utilization in the form of screen-printed film in TENGs. Further, TEM-SAED pattern of La_2O_3 nanocrystals showed high intense diffraction spots conclude that the particles were crystallized. FTIR analysis showed the presence of La–O bond. XPS analysis showed the chemical nature of the nanocrystals. The film of La_2O_3 was investigated for its triboelectric behavior and the results depict that the peak output power density could reach up to 7.125 W/m^2 at load resistor of 30

MΩ. Thus, these results depict that La_2O_3 film TENG device could be used for the self-powered devices and many improvements could be done to improve the power density to use it in various energy harvesting applications.

Acknowledgements

The authors are thankful to Ms. Rashmi for her help taking in SEM micrographs. The authors would also like to thank the "Central Surface Analytical Facility of IIT Bombay" for the assistance in XPS characterization.

Declarations

Conflict of interest The authors have no conflict of interest.

Supplementary Information: The online version contains supplementary material available at https://doi.org/10.1007/s10854-021-06545-7.

References

1. Q. Liang, Q. Zhang, X. Yan, X. Liao, L. Han, F. Yi, M. Ma, Y. Zhang, Adv. Mater. **29**, 1604961 (2017)
2. H.Y. Mi, X. Jing, Q. Zheng, L. Fang, H.X. Huang, L.S. Turng, S. Gong, Nano Energy **48**, 327 (2018)
3. Z. Saadatnia, S.G. Mosanenzadeh, T. Li, E. Esmailzadeh, H.E. Naguib, Nano Energy **65**, 104019 (2019)
4. H.Y. Mi, X. Jing, M.A.B. Meador, H. Guo, L.S. Turng, S. Gong, ACS Appl. Mater. Interfaces **10**, 30596 (2018)
5. Y. Tang, Q. Zheng, B. Chen, Z. Ma, S. Gong, Nano Energy **38**, 401 (2017)
6. H. Wang, M. Shi, K. Zhu, Z. Su, X. Cheng, Y. Song, X. Chen, Z. Liao, M. Zhang, H. Zhang, Nanoscale **8**, 18489 (2016)
7. S.H. Ramaswamy, J. Shimizu, W. Chen, R. Kondo, J. Choi, Nano Energy **60**, 875 (2019)
8. B. Zhang, L. Zhang, W. Deng, L. Jin, F. Chun, H. Pan, B. Gu, H. Zhang, Z. Lv, W. Yang, Z.L. Wang, ACS Nano **11**, 7440 (2017)
9. Z. Saadatnia, S.G. Mosanenzadeh, E. Esmailzadeh, H.E. Naguib, Sci. Rep. **9**, 1370 (2019)
10. J. Sheng, S. Zhang, S. Lv, W. Sun, J. Mater. Sci. **42**, 9565–9571 (2007)
11. A.V. Murugan, A.K. Viswanath, J. Phys. D **39**, 3974 (2006)
12. C.J. Murphy, T.K. Sau, A.M. Gole, C.J. Orendorff, J. Gao, L. Gou, S.E. Hunyadi, T. Li, J. Phys. Chem. B **109**, 13857 (2005)
13. J.W. Stouwdam, G.A. Hebbink, J. Huskens, F.C.J.M. Van Veggel, Chem. Mater. **15**, 4604 (2003)
14. Y. Xiao, Z. Feng, X. Huang, L. Huang, Z. Long, Q. Wang, Y. Hou, Chin. Sci. Bull. **59**, 1864 (2014)
15. P. Allenspach, U. Gasser, J. Alloys Compd. **311**, 1 (2000)
16. J. Zhang, Z. Zhang, Y. Jiao, H. Yang, Y. Li, J. Zhang, P. Gao, J. Power Sources **419**, 99 (2019)
17. Y. Zhou, W. Deng, J. Xu, J. Chen, Cell Rep. Phys. Sci. **1**, 100142 (2020)
18. L. Kong, Y. Tian, N. Li, Y. Liu, J. Zhang, J. Zhang, W. Zuo, Appl. Clay Sci. **162**, 507 (2018)
19. M. Ghiasi, A. Malekzadeh, Superlattices Microstruct. **77**, 295 (2015)
20. Q. Mu, Y. Wang, J. Alloys Compd. **509**, 396 (2011)
21. M. Salavati-Niasari, G. Hosseinzadeh, F. Davar, J. Alloys Compd. **509**, 4098 (2011)
22. P.G.A. Krishna, N.J. Tharayil, *AIP Conf. Proc.* **2162**, 20079 (2019)
23. M. Osada, T. Sasaki, Adv. Mater. **24**, 210 (2012)
24. G.N. Sharma, K.V. Rao, V.S.S. Kumar, C.S. Chakra, V. Rajendar, P.R. Reddy, *IOP Conf. Ser. Mater. Sci. Eng.* **73**, 012099 (2015)
25. M.F. Vignolo, S. Duhalde, M. Bormioli, G. Quintana, M. Cervera, J. Tocho, Appl. Surf. Sci. **197**, 522–526 (2002)
26. S. Sivasankaran, M.J. Kishor Kumar, Ceram. Int. **41**, 11301 (2015)
27. M. Salavati-Niasari, G. Hosseinzadeh, F. Davar, J. Alloys Compd. **509**, 134 (2011)
28. J. Deng, L. Zhang, C.T. Au, H. Dai, Mater. Lett. **63**, 632 (2009)
29. J. Liu, G. Wang, L. Lu, Y. Guo, L. Yang, RSC Adv. **7**, 40965 (2017)
30. W. Nowicki, Z.S. Piskuła, P. Kuźma, P. Kirszensztejn, J. Sol-Gel Sci. Technol. **82**, 574 (2017)
31. C. Hu, H. Liu, W. Dong, Y. Zhang, G. Bao, C. Lao, Z.L. Wang, Adv. Mater. **19**, 470 (2007)
32. F. Khosrow-Pour, M. Aghazadeh, S. Dalvand, B. Sabour, Mater. Lett. **104**, 61 (2013)
33. Q. Liang, X. Yan, Y. Gu, K. Zhang, M. Liang, S. Lu, X. Zheng, Y. Zhang, Sci. Rep. **5**, 9080 (2015)
34. Z. Wen, Q. Shen, X. Sun, Nano-Micro Lett. **9**, 45 (2017)
35. C. Zhang, Z.L. Wang, Micro Electro Mechanical Systems. Micro/Nano Technologies. Springer, Singapore, pp. 1335–1376 (2018)
36. A.S.P. Dewi, N. Mufti, A.A. Fibriyanti, M. Diantoro, A. Taufiq, A. Hidayat, Sunaryono, H. Nur, J. Polym. Res. **27**, 1 (2020)

37. M.R. Sovizi, S. Mirzakhani, New J. Chem. **44**, 4927 (2020)
38. S. Jafari Nejad, H. Abolghasemi, M.A. Moosavian, A. Golzary, M.G. Maragheh, J. Supercrit. Fluids **52**, 292 (2010)
39. A.A. Badawy, S.M. Ibrahim, Int. J. Ind. Chem. **7**, 287 (2016)
40. K. Ngaosuwan, W. Chaiyariyakul, O. Inthong, W. Kiatkittipong, D. Wongsawaeng, S. Assabumrungrat, Catal. Commun. **149**, 106247 (2021)